Earthquake Engineering, Tenth World Conference © 1992 Balkema, Rotterdam. ISBN 90 5410 060 5

Developments in understanding, analysing and designing structures with aseismic isolation

R. Ivan Skinner, Graeme H. McVerry & William H. Robinson
Engineering Seismology Section, DSIR Physical Sciences, Lower Hutt, New Zealand

ABSTRACT: Two aspects of seismically isolated systems are summarised here, namely the effects of the degree of isolation on the modal profiles and periods, and on the seismic motions and loads, of a linearly isolated system, and the effects of isolator nonlinearity, as deduced from a study of 81 cases with varying bilinear and structural parameters. The latter analysis provides an overview of important design parameters, and can be used as a starting point for more detailed aseismic design.

1 INTRODUCTION

This paper presents some of the ideas and techniques discussed at greater length in a forthcoming book, "An Introduction to Seismic Isolation" by the same authors, to be published by John Wiley and Sons. The modal approach to the understanding and evaluation of seismic responses of isolated structures is introduced with reference to the simple case of a continuous uniform shear structure mounted on a linear isolator. Extension of the modal approach to the nonlinear case is discussed in terms of a bilinear isolator.

An isolation factor I which applies for both linear and bilinear isolation is introduced to simplify the presentation of the features of well-isolated natural modes, Figure 1. An isolator nonlinearity factor NL is introduced to simplify the presentation of the maximum seismic responses of modes when the isolator is idealised as bilinear hysteretic. Modal contributions to maximum seismic responses have been evaluated by applying modal filtering techniques to the time-histories of overall seismic responses. Results based on a range of case studies are summarised in Figure 2.

2 LINEAR ISOLATION

The primary effects of a high degree of linear isolation are large reductions in the first mode accelerations and loads, and usually a substantial increase in structural displacements, which now apply at all levels down to the structure-isolator interface. Higher-mode weights are very considerably reduced so that their contributions to seismic loads are usually small. "Floor" spectra are correspondingly reduced at shorter periods.

The degree of modal isolation depends on the ratio between the flexibility of the isolator and the flexibility of the structure. To permit generalisation to non-uniform structures, the flexibility ratio is expressed in terms of a related period ratio as follows:

$$I = T_b / T_1(U)$$

where T_b = isolator natural period when the structure is rigid
$= 2\pi\sqrt{M/K_b}$
and $T_1(U)$ = first natural period of the unisolated structure
$= 4\sqrt{M/K}$ for the uniform shear structure

where M = total structural mass
K_b, K = isolator, overall structural stiffness.
Without isolation, $T_b = 0$, and hence $I = 0$.
With complete isolation, $T_b \rightarrow \infty$ and hence $I \rightarrow \infty$.

The effect of the degree of linear isolation on the features of natural modes, and on their seismic responses, is illustrated in Figure 1, for which the continuous uniform shear structure of Figure 1(a) is adopted. The cyclic load-displacement loop for the isolator natural period T_b has the form shown in Figure 1(a)(i), which includes the affect of viscous damping.

Figure 1(b) shows the normalised mode-n displacement profiles, $\phi_n(z) = u_n(z) / |u_n(L)|$, for no isolation $I = 0$, for intermediate degrees of isolation $I = 2.0$ or 4.0, and for complete isolation $I = \infty$ (the solid lines). By the time the isolation factor I has been increased to 2.0, the mode shapes are already close to their completely isolated profiles. The greatest

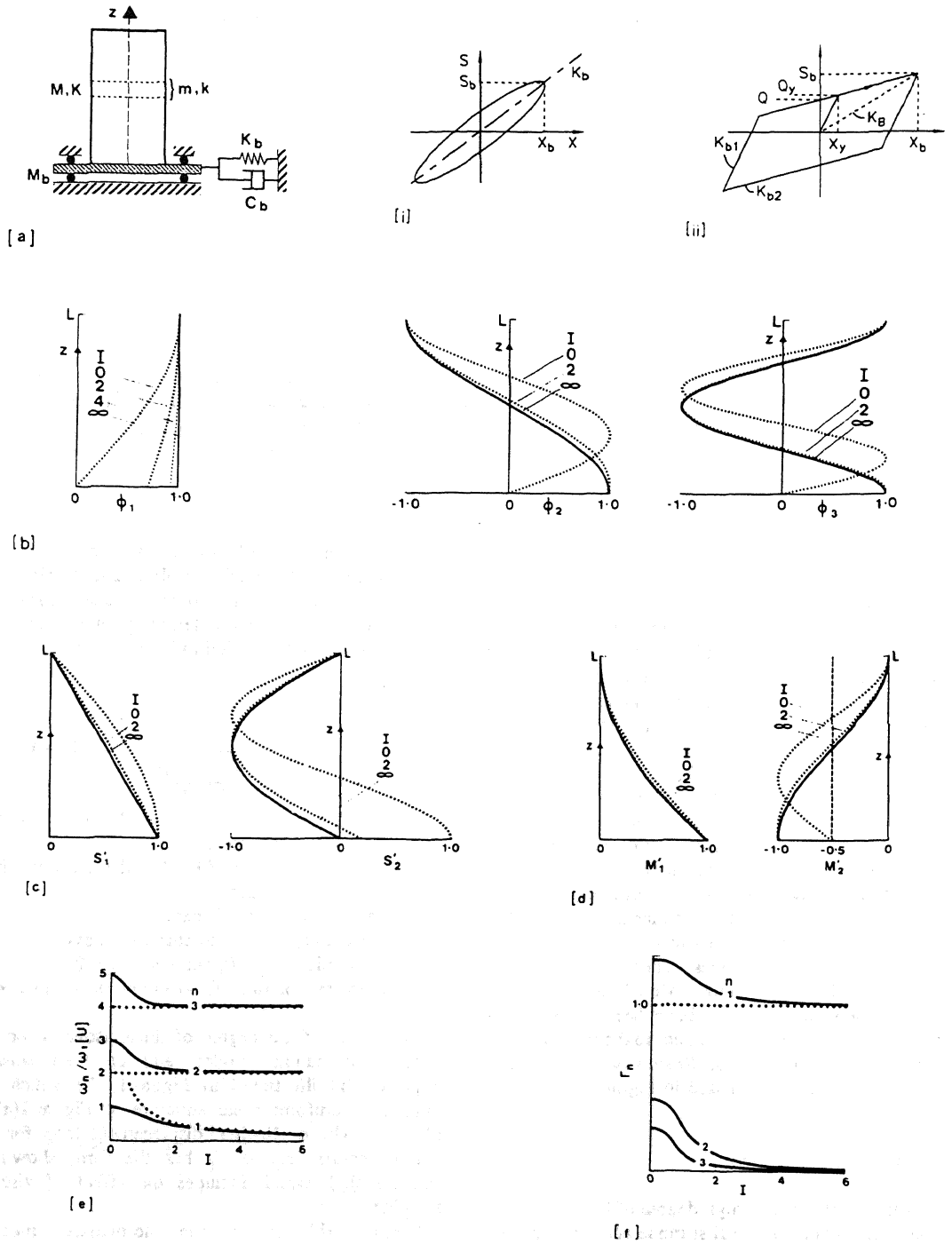

Figure 1: Modal features of an undamped continuous uniform shear structure with degree I of linear isolation.
(a): Model with load-displacement loops for (i) linear spring, (ii) bilinear hysteretic spring.
(b), (c), (d): normalised profiles of displacement ϕ_n, shear S_n, moment M_n.
(e): Frequency ratio, $\omega_n(I)/\omega_1(U)$
(f): Mode weight, $\Gamma_n = |\Gamma_n(L)|$

departure is for the mode-1 profile, which is however very close to the static profile given by mass-proportional forces. Since isolator periods T_b of 2.0 seconds or more are usually chosen to obtain low seismic loads and structural deformations, and sometimes to achieve low floor spectra, an isolation factor I of 2.0 or more results when $T_1(U)$ is 1.0 seconds or less. For such isolation the modal features and seismic responses approach the values or relationships given by a very high degree of isolation, as illustrated by Figures 1(b) to (f). Figure 1(c) gives the normalised shear profiles $S_n(z) = S_n(z) / |S_{n,max}|$, and Figure 1(d) gives the normalised overturning moment profiles $M_n(z) = M_n(z) / |M_{n,max}|$. Figure 1(e) gives the ratios of the isolated modal frequencies $\omega_n(I)$ to the first unisolated modal frequency $\omega_1(U)$; where $\omega_n(I)/\omega_1(U) = T_1(U)/T_n(I)$; asymptotes for the frequency ratios when I is large are shown dotted. The large reduction in the mode-1 period results in a large reduction in the values given by acceleration response spectra and a correspondingly large increase in the values given by displacement response spectra. Figure 1(f) shows the mode weights $\Gamma_n = |\Gamma_n(L)|$, where $\Gamma_n(z)$ (defined for lumped mass structures in (6) below) is the participation factor for mode n at level z.

Maximum seismic responses of the isolated mode n of a general linearly isolated structure with masses m_r at levels z_r can be expressed in the usual way as

$$X_{rn} = \Gamma_{rn} S_D(T_n, \zeta_n) \tag{1}$$

$$\ddot{X}_{rn} \text{ (absolute)} = \Gamma_{rn} S_A(T_n, \zeta_n) \tag{2}$$

$$F_{rn} = m_r \ddot{X}_{rn} \text{ (absolute)} \tag{3}$$

$$S_{rn} = \sum_{i=r}^{n} F_{in} \tag{4}$$

$$M_{rn} = \sum_{i=r+1}^{n} S_{in}(z_{in} - z_{i-1,n}) \tag{5}$$

where

$$\Gamma_{rn} = u_{rn} \frac{\Sigma m_i u_{in}}{\Sigma m_i u_{in}^2} \tag{6a}$$

Here X and $\ddot{X}$ (abs.) refer to peak values of relative displacement and absolute acceleration respectively, S_D and S_A are the displacement and acceleration response spectra, ζ_n is the modal damping factor, and Γ_{rn} are the modal participation factors.

For isolation factors I = 2.0 or more, equations (1) to (5) give approximately correct values when based on completely isolated mode shapes, u_{rno}. However, the numerator summation for Γ_{rn} in (6a) is zero for completely isolated higher modes, n > 1. Γ_{rn} can then be based on the mode shapes with an isolator stiffness K_b. However, it may be convenient to postpone computing accurate mode shapes for given K_b values, in order to evaluate the small differences in the numerator of (6a), and instead to obtain effective higher-mode seismic participation factors from the relationship

$$\Gamma_{rn} \approx \frac{u_{rn} u_{1n} M}{\Sigma m_i u_{in}^2} \left(\frac{T_n}{T_b}\right)^2 \tag{6b}$$

which uses $K_b u_{1n} = \omega_n^2 \Sigma m_i u_{in}$. Since (6b) is not critically dependent on the exact mode shape, it may also use the completely isolated u_{in} values, as can equations (1) to (5) as noted above.

Since the higher-mode participation factors for well-isolated structures are very small, as indicated by the higher-mode weights in Figure 1(f), the higher modes make no significant contribution to the seismic displacements, and small or at most moderate contributions to the seismic loads. Higher modes may, however, make major contributions to the small floor spectra, for periods less than 1.0 seconds, provided the isolation factor I is moderate and the structural and spectral dampings are low. In the special cases where the design calls for very low floor spectra it is necessary to consider the increases in higher-mode participation factors given by high isolator damping.

Detailed perturbation analysis shows that the approximate result of increasing the isolator damping factor, by an amount which is ζ_b above the damping required to give classical damping for mode n, is to multiply the higher-mode participation factors as given by equation (6a) or (6b), by the ratio;

$$\Gamma_{rn}(K_b, C_b)/\Gamma_{rn}(K_b) = \sqrt{1 + (2\zeta_b \omega_n/\omega_b)^2} \tag{6c}$$

It is of interest to note that this is equivalent to replacing the isolator spring force K_b by the modulus of the complex spring force $|K_b + i\omega_n C_b|$ when applying equation (6a) or (6b).

A result of high isolator damping is significantly non-classical higher-mode shapes, with phase changes in the profile of any mode n and some consequent phase changes in the corresponding Γ_{rn} values. As one consequence of the phase changes, it is not strictly correct to perform the summations in equations (4), (5) and (6). However, further studies (as will be detailed in the book), indicate that approximate results may be obtained by neglecting phase change effects (except for their contribution of factor (6c) above) provided I = 2 and ζ_b has values up to about 0.2, or I = 3 and ζ_b has values up to about 0.3. A further consequence of the

modal phase changes is some (probably small) errors which arise from the response spectral values S_D and S_A, which are used in equations (1) and (2).

More accurate modal features, periods, dampings and shapes (and hence more accurate values for the modal seismic responses derived from them by equations (1) to (6)) may be obtained by adding small correction or perturbation terms to the values given by assuming complete isolation, or a rigid structure in the case of isolated mode 1. Such perturbation terms are essential for evaluating the small higher-mode participation factors, which are zero when the structure is completely isolated. The first-mode participation factors may be approximated by 1.0, as given by a rigid structure, or more accurately by substituting the static displacements in (6a).

3 NON-LINEAR ISOLATION

The primary effects of non-linearity of the isolation are different (and less easily defined) seismic response spectra for the first mode, and different and sometimes much larger weights for the seismic responses of higher modes. A design task is to relate the isolator parameters to those of the structure in such a way that higher-mode responses are limited to acceptable levels. The analysis summarised below provides an overview of important design parameters and can be used as a starting point for more detailed analyses of specific structures.

The seismic responses of a linear structure with a bilinear isolator are controlled by two sets of natural modes and the interactions between them. The first (elastic-phase) set of modes is given by the structure when the isolator stiffness is K_{b1}. The second (yielded-phase) set of modes is similarly given by the structure with an elastic isolator stiffness K_{b2}. The yield level ratio Q_y/W plays an important role in the interaction between the elastic-phase and yielded-phase mode sets, including the degree of excitation of the higher modes of the yielded mode set. Each mode set has an isolation factor given respectively by:

$$I(K_{b1}) = T_{b1}/T_1(U); \quad I(K_{b2}) = T_{b2}/T_1(U) \qquad (7)$$

where

$$T_{b1} = 2\pi\sqrt{M/K_{b1}}\ ; \quad T_{b2} = 2\pi\sqrt{M/K_{b2}} \qquad (8)$$

Since the maximum seismic responses typically occur during the yielded isolator phase, the distributions of maximum modal responses are given by yielded-phase mode shapes. The response distributions for the uniform shear structure are again illustrated by Figure 1 (b) (c) and (d) with the isolation factor now given by $I(K_{b2})$.

The elastic-phase isolation factor $I(K_{b1})$ and the non-linearity factor NL, for which the yield ratio is an essential parameter, combine to play an important role in the strengths of the yielded-phase higher mode responses as discussed below.

The dashed curves in Figure 2(a) show the base shear-to-weight ratio S_b/W as a function of the effective mode-1 period $T_B = 2\pi\sqrt{M/K_B}$ (i.e. for a rigid structure, and with K_B defined in Figure 2(c)) and as a function of the effective damping $\zeta_B(\%)$. The solid lines show the corresponding peak displacements X_b. These curves were obtained from a "bilinear dataset" (81 cases given by three values of each of the parameters T_{b1}, T_{b2}, Q_y/W, $T_1(U)$). The correction factor C_F, as given in Figure 2(b), has been included in the vertical scales of Figure 2(a) as without C_F there are substantial departures from the curves for some combinations of isolator parameters.

The effective period T_B and the damping factor ζ_B can be related to properties of the bilinear loop using Figure 2(c), which is based on the bilinear hysteresis loop of Figure 1(a)(ii). A useful measure of the non-linearity of a bilinear loop is the ratio NL = OP/S_b (see Figure 2(c)), which becomes unity when the loop is rectangular and zero if there is no hysteresis. Because the nonlinearity is proportional to the ratio between the areas of the hysteresis loop and a circumscribing rectangle ($4S_bX_b$), NL is simply related to the hysteretic damping, so that $\zeta_h = (2/\pi)$NL. Where isolator velocity-damping (ζ_b) is included, the effective isolator damping is given by $\zeta_B = \zeta_b + \zeta_h$. While the nonlinearity and ζ_h are constant for any yield point such as J on the dashed line PR, locations near R give large values of T_{b2}, which should be avoided (see below). Similarly, when the yield point J is close to P, T_{b1} is small and it is difficult to obtain a small ratio $T_1(U)/T_{b1}$ and hence to suppress higher-mode excitations (see below).

For the rectangular-profile approximation to mode 1, the base shear ratio S_b/M equals the peak mode-1 accelerations $\ddot{X}_{r,1}$ (Figure 2(a)). For a 5-storey structure the peak higher-mode acceleration ratio $\ddot{X}_{5,n}/\ddot{X}_{5,1}$ varies with the nonlinearity NL and the period ratio $T_1(U)/T_{b1}$, as shown in Figure 2(d). (Some data points for $T_{b2} = 6.0$ seconds lie well off these lines, with departures following systematic trends.) Since $T_1(U)/T_{b1} = 1/I(K_{b1})$, Figure 2(d) shows that increasing the elastic-phase isolating factor $I(K_{b1})$ reduces the ratio of higher-mode to mode-1 maximum accelerations; for a given degree of non-linearity NL. Hence increasing the elastic-phase isolation, or reducing the non-linearity, generally reduces the degree of higher-mode excitation. If the ratio $T_1(U)/T_{b1}$ is small then the structure is effectively rigid. It is evident that an effectively rigid structure would have little higher-mode excitation.

Figure 2(e) shows the variation, with height up the building, of the shear due to mode 1 alone, namely $S_{r,1}$

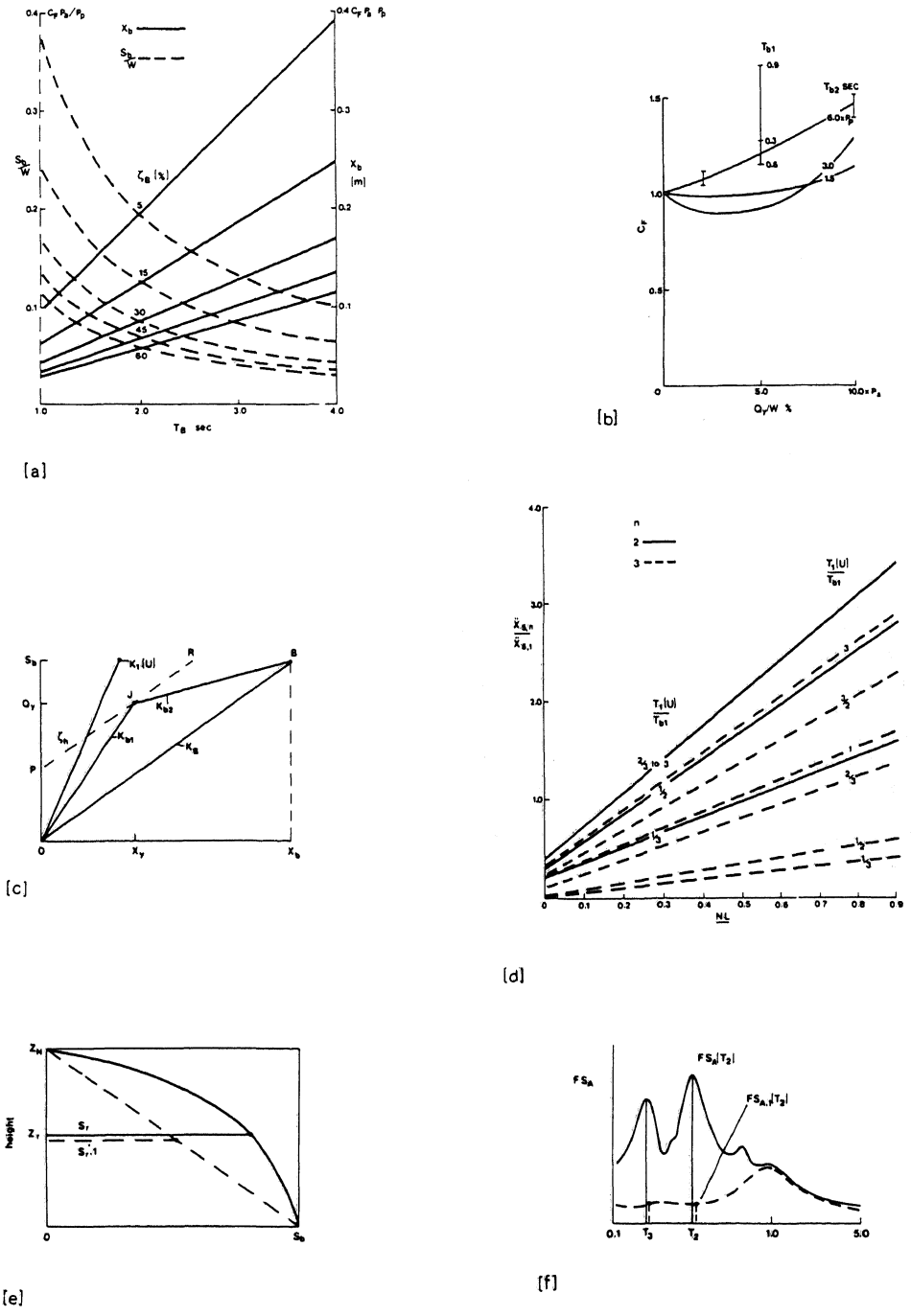

Figure 2: Seismic responses of a 5-storey uniform shear structure with a bilinear isolator (Figure 1(a)(ii)), for scaled El Centro NS 1940 earthquake.

(a): Maximum shear force S_b and displacement X_b at the structure-isolator interface.

(b): Correction factor, C_F.

(c): Bilinear parameters controlling T_B and ζ_B.

(d): Ratios of peak modal accelerations at the top level.

(e): Shear bulge factor at level r, $\underline{BF}_r = S_r/S_{r,1}$.

(f): Contributions of modes to floor spectra.

(dashed line) as well as the total seismic force S_r (solid line). The contribution of higher modes may be represented as a shear bulge factor $\underline{BF}_r = S_r/S_{r,1}$ as introduced by Lee and Medland (Earthq. Eng. and Struct. Dyn. 7 (1979) 555). The dataset (81 cases) gives approximate values for near-midheight bulge factors as

$$\underline{BF}_r \approx \sqrt{1 + 0.9\left(\ddot{X}_{N,2}/\ddot{X}_{N,1}\right)^2} \quad . \tag{9}$$

Since $\ddot{X}_{N,2}/\ddot{X}_{N,1}$ is given approximately by Figure 2(d) for $N = 5$, it is clear that higher nonlinearity, combined with high values of the ratio $T_1(U)/T_{b1}$ (low elastic-phase isolation), tend to produce substantial shear bulge factors.

While the higher-mode acceleration responses of Figure 2(d) and the shear bulge factors of equation (7) give quantitative approximations to maximum seismic responses for a uniform shear structure, the value become increasingly approximate, but still give general guidelines, for increasingly irregular or non-shear type structures.

Figure 2(f) shows the general effect of higher modes on the floor acceleration spectra $\underline{FS}_A$. This has been drawn for cases where $\ddot{X}_{N,n}/\ddot{X}_{N,1}$ is of the order of unity, see Figure 2(d). The ratio of the total floor spectra (solid line) to the mode-1 floor spectra (dashed line) shows that higher-mode accelerations dominate for shorter spectral periods ($T < 1.0$ s).

It is therefore clear that non-linearity, if not suppressed by a high elastic-phase isolation factor $T_{b1}/T_1(U)$, can give rise to substantial higher-mode contributions to seismic loads and to large increases in the floor acceleration spectra at shorter periods ($T < 1.0$ s).